Impaired eIF5A function causes a Mendelian disorder that is partially rescued in model systems by spermidine

Víctor Faundes[1,2], Martin D. Jennings[3,4], Siobhan Crilly[5], Sarah Legraie[1], Sarah E. Withers[5], Sara Cuvertino[1], Sally J. Davies[6], Andrew G.L. Douglas[7,8], Andrew E. Fry[6,9], Victoria Harrison[7], Jeanne Amiel[10,11,12], Daphné Lehalle[10], William G. Newman[1,13], Patricia Newkirk[14], Judith Ranells[14], Miranda Splitt[15], Laura A. Cross[16,17], Carol J. Saunders[18,19,20], Bonnie R. Sullivan[16,17], Jorge L. Granadillo[21], Christopher T. Gordon[11,12], Paul R. Kasher[4,5], Graham D. Pavitt[3,4], Siddharth Banka[1,13].

1. Division of Evolution & Genomic Sciences, School of Biological Sciences, Faculty of Biology, Medicine and Health, University of Manchester, Manchester M13 9PT, United Kingdom.
2. Laboratorio de Genética y Enfermedades Metabólicas, Instituto de Nutrición y Tecnología de los Alimentos (INTA), Universidad de Chile, Santiago 7830490, Chile.
3. Division of Molecular and Cellular Function, School of Biological Sciences, Faculty of Biology, Medicine and Health, University of Manchester, Manchester M13 9PT, United Kingdom.
4. Manchester Academic Health Science Centre, University of Manchester, Manchester M13 9WL, United Kingdom.
5. Division of Neuroscience & Experimental Psychology, School of Biological Sciences, Faculty of Biology, Medicine and Health, University of Manchester, Manchester M13 9WL, United Kingdom.
6. Institute of Medical Genetics, University Hospital of Wales, Heath Park, Cardiff CF14 4XW, United Kingdom.

7. Wessex Clinical Genetics Service, Princess Anne Hospital, Southampton SO16 5YA, United Kingdom.
8. Human Development and Health, Faculty of Medicine, University of Southampton, Southampton General Hospital, Southampton SO16 6YD, United Kingdom.
9. Division of Cancer and Genetics, School of Medicine, Cardiff University, Cardiff CF14 4XN, United Kingdom
10. Department of Genetics, AP-HP, Hôpital Necker Enfants Malades, 75015 Paris, France.
11. Laboratory of Embryology and Genetics of Human Malformations, INSERM UMR 1163, Institut Imagine, 75015 Paris, France.
12. Paris Descartes-Sorbonne Paris Cité University, Institut Imagine, 75015 Paris, France.
13. Manchester Centre for Genomic Medicine, St Mary's Hospital, Manchester University NHS Foundation Trust, Health Innovation Manchester, Manchester M13 9WL, United Kingdom.
14. Division of Genetics and Metabolism, Department of Pediatrics, University of South Florida, Tampa, Florida 33606, United States of America.
15. Northern Genetics Service, Institute of Genetic Medicine, Newcastle upon Tyne NE1 3BZ, United Kingdom.
16. Division of Clinical Genetics, Children’s Mercy—Kansas City, Missouri 64108, USA
17. Department of Pediatrics, University of Missouri—Kansas City, Kansas City, Missouri 64108, USA.
18. Center for Pediatric Genomic Medicine Children’s Mercy–Kansas City, Missouri 64108, USA;
19. School of Medicine, University of Missouri–Kansas City, Kansas City, Missouri 64108, USA;

20. Department of Pathology and Laboratory Medicine, Children's Mercy–Kansas City, Missouri 64108, USA;

21. Division of Genetics and Genomic Medicine, Department of Pediatrics, Washington University School of Medicine, St. Louis, Missouri. United States of America.

Correspondence

Dr Siddharth Banka

Manchester Centre for Genomic Medicine

St Mary's Hospital

Manchester M13 9WL

United Kingdom

Tel: +44 (0) 161 70 10980; Fax: +44 (0) 161 27 66145

siddharth.banka@manchester.ac.uk

Or

graham.pavitt@manchester.ac.uk

Or

paul.kasher@manchester.ac.uk

Abstract

The structure of proline prevents it from adopting an optimal position for rapid protein synthesis. Polyproline-tract (PPT) associated ribosomal stalling is resolved by highly-conserved eIF5A, the only protein to contain the amino acid, hypusine. We show that *de novo* heterozygous *EIF5A* variants cause a disorder characterized by variable combinations of developmental delay, microcephaly, micrognathia and dysmorphism. Yeast growth assays, polysome profiling, total/hypusinated eIF5A levels and PPT-reporters studies reveal that the variants impair eIF5A function, reduce eIF5A-ribosome interactions and impair the synthesis of PPT-containing proteins. Supplementation with 1 mM spermidine partially corrects the yeast growth defects, improves the polysome profiles and restores expression of PPT reporters. In zebrafish, knockdown *eif5a* partly recapitulates the human phenotype that can be rescued with 1 μM spermidine supplementation. In summary, we uncover the role of eIF5A in human development and disease, demonstrate the mechanistic complexity of *EIF5A*-related disorder and raise possibilities for its treatment.

Introduction

Proline is a unique amino acid as its amine nitrogen is bonded to two, instead of one, carbon atoms with a distinctive rigid cyclic structure that prevents it from adopting an optimal position required for rapid protein synthesis[1]. The presence of proline, either as a peptidyl donor or acceptor, impedes the rate of peptide bond formation by the ribosome, an inhibitory effect that becomes progressively stronger, to the extent that three or more consecutive prolines provoke ribosome stalling[2-4]. In eukaryotic cells, ribosomal stalling is resolved by the Eukaryotic Translation Initiation Factor 5A (eIF5A), which is critical for the synthesis of peptide-bonds between consecutive proline residues[5]. Notably, the frequency of poly-proline tracts (PPTs) is higher in evolutionarily new proteins and of all tandem amino acid repeats, only the proline repeat frequency correlates with functional complexity of eukaryotic organisms[6]. eIF5A1 (hereafter eIF5A) and its normally undetectable paralogue eIF5A2 are the only human proteins that contain the amino acid hypusine, a post-translationally modified lysine at position 50 (K50)[2-4]. Hypusine is synthesized from spermidine, a polyamine, via two sequential enzymatic steps involving highly conserved deoxyhypusine synthase (DHPS) and deoxyhypusine hydroxylase (DOHH) enzymes[7]. Hypusinated eIF5A stabilizes P-tRNA that facilitates peptide bond formation at stalled ribosomes[5]. Other functions of eIF5A include recognition of the correct start codon[8,9], global protein synthesis elongation and termination[10,11], promoting the elongation of many non-polyproline-specific tripeptide sequences, and eliciting nonsense-mediated decay (NMD)[12]. It is essential for cell viability and growth in both simple[2,5] and complex[3] organisms. Somatic overexpression of *EIF5A* has unfavourable prognostic implications in several cancers including pancreatic, lung, hepatocellular, bladder and colorectal carcinomas[13,14]. However, no human phenotype has been previously attributed to germline *EIF5A* variants.

Here, we demonstrate that *de novo* heterozygous *EIF5A* variants cause a previously undescribed syndrome characterised by variable combinations of developmental delay, microcephaly, micrognathia, congenital malformations and dysmorphism. These variants likely result in the loss of eIF5A function through distinct mechanisms and lead to impaired interaction between eIF5A and ribosomes. Both functional and phenotypic consequences of impaired eIF5A activity are partially rescued by spermidine supplementation in yeast and zebrafish models.

Results

Germline variants in *EIF5A* cause a previously undescribed craniofacial-neurodevelopmental disorder

In an individual with intellectual disability, congenital microcephaly, micrognathia and clinical suspicion of a Kabuki syndrome (MIM # 147920)-like condition[15], we identified a *de novo* heterozygous frameshift variant in *EIF5A* (c.324dupA, p.R109Tfs*8) by trio whole exome sequencing (Figure 1a-c, Table 1, individual #3, Supplementary Note 1). *EIF5A* has 4 protein-coding transcripts, but ENST00000336458/NM_001970.5 (Uniprot P63241) is preferentially, widely and most highly expressed in all adult human tissues[16-18]. Only one truncating variant has been recorded in gnomAD, a variant sequence database of >140,000 control individuals, in this transcript (gnomAD o/e_{LoF}=0.11; pLI = 0.74)[19]. Also, the GeVIR metrics (GeVIR AD = 4.38; VIRLoF AD = 2.21) add supportive evidence that *EIF5A* is highly likely to be associated with autosomal dominant disease[20]. Hence, we concluded that the *EIF5A* variant identified in individual #3 was significant. Through Matchmaker Exchange[21] and GeneMatcher[22] we identified six additional individuals with nonsense or missense *de novo EIF5A* variants (c.143C>A, p.T48N; c.316G>A, p.G106R; c.325C>G, p.R109G; c.325C>T, pR109*; c.343C>T, p.P115S; c.364G>A, p.E122K). The missense

variants are located in one of the most constrained coding regions of the human genome (>99th percentile)[23], and affect residues that are highly evolutionarily conserved (Fig. 1b and c). *In-silico* modelling of missense variants (Fig. 1d) onto the structure of yeast eIF5A in complex with the 60S ribosome (PDB entry 5GAK)[24] shows that the missense variants affect surface-exposed residues. T48 is adjacent to the hypusinated lysine 50, G106 and R109 residues are close to the ribosomal protein uL1 and E122 is close to the P-site tRNA. In contrast P115 has no clear intermolecular interactions. Although the individuals were identified via their genotypes, on reverse phenotyping[25] their clinical features showed remarkable convergence. All patients were affected by variable degrees of developmental delay and/or intellectual disability, microcephaly (either absolute or relative) and overlapping facial dysmorphisms (Table 1, Fig. 1a, Supplementary Note 1). Notably, four individuals in this cohort were clinically suspected to have either a Kabuki syndrome-like or a mandibulofacial dysostosis (MIM #154400) -like condition (Table 1, Supplementary Note 1). *eif5a/Eif5a* mRNA is highly expressed in *Danio rerio* (hereafter zebrafish)[26] and *Mus musculus*[27] (hereafter mouse) embryos in structures that form the brain and mouth, thus corresponding with the most significantly impacted structures in the affected individuals. Overall, these results are strongly indicative of the frameshift, nonsense and missense *EIF5A* variants being causal for the phenotypes of the affected individuals.

EIF5A **variants impair eIF5A function**

Peripheral blood mononuclear cells obtained from Individual 3, with the *EIF5A* frameshift variant c.324dupA, and two healthy controls were transformed by Epstein-Barr virus into lymphoblastoid cell lines (LCLs). Blood samples from other affected individuals were not available. The *EIF5A* mRNA level in LCLs was significantly reduced in Individual 3 (Fig.

156 1e) and the transcript with c.324dupA was not detected (Supplementary Figure 1), suggesting
157 NMD of the mutant transcript.
158
159 The *Saccharomyces cerevisiae* (yeast) and human eIF5A share a very high degree of
160 conservation (62% identity/ 92% similar) (Fig. 1b) and well-established assays to investigate
161 eIF5A function in yeast are available[2,5]. We synthesised a human *EIF5A* cDNA (*h*eIF5A
162 hereafter) optimised for yeast codon usage, and added the 5' and 3' control regions of the
163 yeast homolog of *EIF5A* (known as *TIF51A* or *HYP2*, *y*eIF5A hereafter) (Supplementary
164 Note 2 and Supplementary Table 1). Introduction of this construct on a centromeric plasmid
165 using standard techniques in a yeast strain in which both *TIF51A* and *TIF51B* (a second
166 *y*eIF5A gene that is transcribed only in anaerobic conditions[2]) are deleted (Supplementary
167 Table 3 and Supplementary Figure 2) restored its growth potential similar to the wild type
168 *y*eIF5A (Fig. 2a, rows 1 and 3). This confirmed that the synthetic *h*eIF5A can replace *y*eIF5A
169 functions in line with previous reports[28].
170
171 Next, we performed site-directed mutagenesis to create *h*eIF5A constructs with the p.T48N,
172 p.G106R, p.R109Tfs*8 and p.E122K variants in centromeric plasmids (Supplementary
173 Tables 1 and 2). The individuals with the p.R109G, p.R109* and p.P115S variants were
174 identified after experiments for other variants were concluded and, therefore, these variants
175 were not included in the functional studies. Yeast colonies expressing the *h*eIF5A-R109Tfs*8
176 as the sole-source of eIF5A could not be obtained after ten days of growth, and across
177 multiple plasmid shuffling experiments (Supplementary Figures 2 and 3). Western blotting
178 using a monoclonal anti-human eIF5A and an anti-hypusinated eIF5A antibody (hereafter
179 hypusine) of pre-shuffled *h*eIF5A-R109Tfs*8 strains co-expressing *h*eIF5A-WT revealed that
180 p.R109Tfs*8 was poorly expressed, and even when expressed in high-copy it was very

poorly hypusinated (Supplementary Figure 4). The poor expression of this mutant in yeast is consistent with our inability to detect this protein in LCLs from individual 3. In contrast, the three missense mutations each supported yeast growth as the sole source of eIF5A showing that they retain sufficient eIF5A function for cell viability. The *h*eIF5A-T48N and *h*eIF5A-G106R yeast cells exhibited slow growth (Fig. 2a, rows 4 and 5), similar to a previously characterised temperature-sensitive mutant *y*eIF5A-S149P mutant (Fig. 2a, row 2)[2,5]. No significant difference was observed between growth of *h*eIF5A-E122K and *h*eIF5A-WT (Fig. 2a, rows 6). These results indicate that the p.T48N and p.G106R variants result in partial loss of eIF5A function, and p.R109Tfs*8 variant results in complete loss of viability. However, the impact of the p.E122K variant remained uncertain.

EIF5A **variants reduce eIF5A-ribosome interaction through different mechanisms**

Next, we asked if the missense variants affected interaction of *h*eIF5A with ribosomes through polysome profiling (Supplementary Figure 5). All missense variants that were tested, including the p.E122K variant, exhibited aberrant polysome profiles, with elevated polysome-to-monosome (P/M) ratios and an increase in the free 60S peak heights and the 60S/80S ratios (Fig. 2c), consistent with a global translation elongation defect [2,5]. Probing for eIF5A and hypusine across polysome fractions revealed that WT eIF5A has ribosome-free (lanes 1-2 in Fig. 2c) and 80S (lane 6 in Fig. 2c) peaks. In contrast, each missense mutant showed a reduction in the 80S ribosome fraction (Fig. 2c), indicating a reduction in ribosome binding by each mutant eIF5A, consistent with the idea that impaired eIF5A-ribosome interactions impact translation elongation of each mutant.

To explore possible mechanisms for the reduction in ribosome binding of missense variants, we performed western blotting. In cells expressing *h*eIF5A-T48N, levels of total eIF5A were

normal, but levels of hypusination were reduced, suggesting that the p.T48N impairs hypusination of the adjacent K50 residue. As hypusination is necessary for eIF5A function, reduced hypusination may contribute to the observed reduction in ribosome association. In contrast total levels of eIF5A were modestly reduced in *h*eIF5A-G106R and *h*eIF5A-E122K cells, while hypusination was unaffected (Fig. 2b). Overall, these results indicated that *EIF5A* variants reduce eIF5A-ribosome interaction, likely through different mechanisms.

***EIF5A* variants impair synthesis of proteins with poly-proline tracts**

Next, we examined if impaired eIF5A function impacted on translation of specific mRNAs. Because eIF5A is especially critical for the optimal synthesis of proteins containing PPTs,[2,5] we studied expression of two previously described PPT reporters – a haemagglutinin (HA)-tagged Ldb17 with a single long PPT of 9 consecutive prolines and HA-Eap1 with 3 shorter PPTs (Supplementary Tables 1 and 3, Fig. 2d).[5] As these reporters require expression with galactose as a carbon source, we first evaluated whether levels of eIF5A and hypusination in these cell growth conditions were consistent with our previous findings. Here in both of the slow-growing mutants (p.T48N and p.G106R) expression of eIF5A was lower than WT. As previously, hypusination was consistently low for p.T48N (Supplementary Figure 6 and 7). By western blotting of total cell extracts we observed decreased levels of both PPT reporters for the p.T48N and p.G106R alleles (Fig. 2d). Although levels of Ldb17 in the p.E122K variant were typically lower than in WT cells, this did not reach statistical significance (Fig. 2d, and Supplementary Figure 7). Hence, the human eIF5A variants impair the synthesis of proteins containing PPTs in yeast.

Human microcephaly-associated genes are enriched for poly-proline tracts

Next, we explored if impaired synthesis of proteins with PPTs could help explain microcephaly, which was the most consistent feature of our patients. To study this, we prepared a catalogue of all known human microcephaly-associated genes (MAGs) according to OMIM and assessed their PPT content[29,30] (Supplementary Table 4). We observed that 198/685 (28.9%) MAGs and 4366/17981 (24.2%) of all other human protein-coding genes have ≥1 PPT [χ^2 7.64; OR=1.27; 95% CI 1.07-1.5; *P*=0.0057]). Next we ranked MAGs according to their proline content in PPTs (Supplementary Table 4, Fig. 2e). *KMT2D* was ranked as #1 in this list. Loss-of-function *KMT2D* variants cause Kabuki syndrome[31], which was the clinically suspected diagnosis in three individuals. *SF3B4,* variants in which cause acrofacial dysostosis 1, Nager type[32] (phenotypic overlap with the clinical suspicion in individual 1), was ranked #5 (Table 1, Fig. 2e).

Spermidine partially rescues impaired eIF5A function in yeast

Polyamines contribute to the efficiency and fidelity of protein synthesis, and spermidine may overcome absence of eIF5A to some extent to promote peptide synthesis [33]. Furthermore, DHPS mediated transfer of a 4-aminobutyl moiety from a polyamine, spermidine, to K50 is the first step in formation of active hypusinated eIF5A[34]. Previous work has demonstrated that spermidine promotes longevity in yeast, whereas depletion of polyamines has a deleterious effect[35]. We therefore reasoned that spermidine supplementation could potentially overcome the effects of impaired eIF5A function. In addition, because p.T48N hypusination was reduced, it may indicate that polyamine concentrations were limiting for hypusination in our growth conditions. We screened the effect of supplementing growth medium with different concentrations of spermidine on yeast growth, as measured by the rate of colony formation (Fig. 3a, Supplementary Figure 8). 1 mM spermidine partially corrected the growth

defects of p.T48N and p.G106R cells (Fig. 3a). As a growth phenotype was not observed in yeast expressing the p.E122K variant, this assay was uninformative for this allele. Higher spermidine concentrations had progressively deleterious effects impairing the growth of all strains (Fig. 3a, Supplementary Figure 8).

Next, we performed polysome profiling of WT, p.T48N and p.G106R cells in presence of 1 mM spermidine. Spermidine treatment improved the global polysome profiles for both mutant strains with no impact on *h*eIF5A-WT (compare Fig. 3b with Fig. 2c). We observed full or partial restoration of *h*eIF5A interaction with the 80S ribosome in p.T48N and p.G106R cells, respectively (Fig. 3b). Furthermore, 1 mM spermidine restored expression of PPT reporter in both growth-rescued mutants (Fig. 3c, left graph). However, improved growth and protein synthesis was not explained by improved eIF5A expression levels or by enhanced hypusination of p.T48N mutant eIF5A (Fig. 3c, middle and right graph). These results suggest that spermidine can rescue and/or bypass impaired eIF5A functions in protein synthesis independent of its role as a substrate for hypusination of eIF5A K50[33].

Spermidine partially rescues phenotypes of impaired eIF5A function in a zebrafish model

We next investigated if spermidine can rescue the impact of loss of eIF5A function in a developing vertebrate model. Zebrafish *eif5a* shares a high degree of conservation with its human orthologue (74% identity, 86% similarity) (Fig. 1b). Previous studies have demonstrated that morpholino-mediated knockdown of *eif5a* or transient overexpression of human *EIF5A* can cause microcephaly in zebrafish larvae[36]. We used a validated and published splice site morpholino (MO)[36] to knockdown *eif5a* in fertilised nacre[37] zebrafish eggs, which were incubated in a standard, spermidine-free medium. The resulting larvae were

fixed and cartilage was stained at 77 hours post-fertilisation (hpf). In line with the human disorder phenotypes, we measured the distance between irises (translating to head circumference and therefore serving as a model for microcephaly), and the length of mandible cartilages (translating to mandibular growth and therefore serving as a model for micrognathia) (Fig 4a, left and right photographs, respectively). Although we did not recapitulate the previously described microcephaly phenotype[36] (Fig. 4b, and Fig. 4c, left graph), the *eif5a* MO induced micrognathia in zebrafish larvae (Fig 4b and Fig. 4c, right graph). Next, we explored the effects on zebrafish of supplementation with 10-fold dilutions (from 1 mM to 0.1 µM) of spermidine. 100 µM or higher concentrations killed larvae before fixation. Supplementation with 1 µM spermidine resulted in partial rescue of micrognathia when compared to control MO (Fig 4b and Fig. 4c, right graph), demonstrating that spermidine supplementation can rescue this developmental defect by bypassing loss of eIF5A. Thus, endogenous concentrations of spermidine within the yolk are not sufficient to overcome loss of eIF5A and spermidine supplementation is likely able to promote peptide synthesis to rescue this developmental defect[33].

Discussion

EIF5A is a unique and critical gene for synthesis of proteins, especially those with PPTs. It is highly intolerant to variation, but so far no human condition caused by variants in this gene has been identified. We define a previously undescribed human disorder caused by heterozygous *EIF5A* variants. This is supported by high constraint for deleterious *EIF5A* variants in population databases, the *de novo* nature of all the variants described here, their absence from population databases along with high evolutionary conservation and the phenotypic similarity of patients ascertained via their genotypes (Fig. 1a-c). The disorder can be caused by protein truncating or missense variants. Of note, the codon encoding Arg109

was impacted in three out of seven cases. In humans, this amino acid is encoded by a CpG including codon (CGA) that may be prone to methylation, deamination and CG-TA transition, each of which could explain clustering of the mutations seen in this study[38]. The phenotype of the condition consists of variable degrees of developmental delay, intellectual disability, microcephaly, and craniofacial dysmorphism, including micrognathia (Table 1, Fig. 1a, Supplementary Note 1). Although both *EIF5A* and *EIF5A2* are hypusinated and widely expressed in adult human tissues, the expression of the former is ~20-fold higher in brain structures than the latter[16]. While *Eif5a*$^{gt/gt}$ mice are embryonically lethal[3], *Eif5a2*$^{-/-}$ mice are viable and display normal development[39]. Therefore, *EIF5A2* expression may not be sufficient to compensate the loss of *EIF5A* function[16]. Pathogenic variants in eIF2B subunits (*EIF2B1*, *EIF2B2*, *EIF2B3*, *EIF2B4* and *EIF2B5*; MIM #603896)[40], *EIF2S3* (MIM #300148)[41], *EIF3F* (MIM # 618295)[42], *EIF4E* (MIM #615091)[43-45] and *EIF4G1* (MIM #614251)[46] have been previously described to cause distinct neurological disorders. Our findings add to this list of translation factors implicated in human developmental disorders.

Yeast growth assays showed the deleterious nature of the truncating and p.T48N and p.G106R missense *EIF5A* variants (Fig. 2a). Our results with the truncating variant are concordant with a previous study that demonstrated that deletion of either eIF5A amino- or carboxy-termini were lethal in yeast[28]. For all studied missense variants, including the E122K variant, the polysome profiles were abnormal further indicating their deleterious nature. More specifically, the higher P/M ratios typically indicate a reduction in translation elongation rates or pausing of ribosomes causing 'traffic jams' on individual mRNAs leading to increased ribosome accumulation on mRNAs. The increase in the free 60S peak heights and the 60S/80S ratios (Fig. 2c) suggests that *EIF5A* missense variants may result in delay of 60S joining during initiation, or reduce the stability of 80S complexes. Both defects are consistent

with the known functions of eIF5A in stimulating the first peptide bond formation and later during elongation and demonstrate clearly that each eIF5A missense mutation impacts protein synthesis globally[2].

Absence of the mutant transcript with the c.324dupA variant and lower level of *EIF5A* mRNA levels in the LCLs of individual 3 suggest haploinsufficiency as the underlying mechanism for the protein truncating variant. This is supported by phenotypic overlap of intellectual disability, microcephaly and retrognathia in patients with 17p13.1 microdeletions that encompass *EIF5A*[47]. Notably, the minimum critical region of this 17p13.1 microdeletion syndrome includes 17 protein-coding genes and its main phenotypic driver has not been resolved. Our observations suggest that haploinsufficiency of *EIF5A* could be responsible for the phenotype of 17p13.1 microdeletion syndrome.

The loss of function of the *EIF5A* missense variants is likely to be due to different mechanisms. The observation of reduced hypusination in cells expressing the p.T48N variant suggests that this variant impairs hypusination of the adjacent K50 residue. Other missense mutations changing residues adjacent to K50 also have reduced hypusination[28], consistent with the idea that they impair interactions with DHPS and/or DOHH enzymes responsible for hypusination. This is also supported by our spermidine supplementation experiment (Fig. 3) that showed no improvement of p.T48N hypusination, indicating that spermidine levels are not a limiting factor for hypusination of this mutant. The DHPS molecular structure indicates that the surface surrounding its active site tunnel is highly acidic[48], while the eIF5A surface region around K50 has a complementary positive charged. *In silico* modelling (Fig. 1d) of the variant structure suggests T48N modestly increases the positive charge, but if or how this affects DHPS or DOHH interactions with eIF5A will require further experimentation.

Reduction of total eIF5A levels in mutant cells (Fig. 2b, and 3c) could be indicative of reduced protein or mRNA stability, but reduced protein levels *per se* are unlikely sufficient to explain the mutant phenotype. Instead our polysomal profile results are indicative of reduced interaction of eIF5A with ribosomes (Fig. 2c) as the common mechanism in the yeast model. As we did not have access to patient cells we could not test mRNA and protein expression levels or functional changes in individuals with the missense variants. Therefore we cannot rule out that other mechanisms such as abnormal splicing or mRNA degradation may contribute to the disorder in individuals with missense *EIF5A* variants. Identification of more individuals in the future with disease-causing variants in this gene will be of great interest to uncover the underlying mechanisms.

We demonstrated that the loss of eIF5A function resulting from the variants has a deleterious impact on synthesis of proteins with PPT (Fig. 2d). The reduction was statistically significant for p.T48N and p.G106R variants. Although we did observe a reduction for the p.E122K variant, it did not reach statistical significance. In all our assays p.E122K was the least affected mutant. This is consistent with the milder individual phenotype of the patient harbouring this variant (Table 1 and Fig. 1a). Human *KMT2D* and *SF3B4* are two MAGs that encode proteins with one of the highest number of PPTs (Fig. 2e). Interestingly, the phenotypes resulting from their loss of function resemble that of the individuals with *EIF5A* variants. From these data we surmise that impaired synthesis of proteins enriched in PPTs such as *KMT2D* and *SF3B4* may underlie the phenotype(s) caused by defective eIF5A. Genes encoding the highest level of polyprolines display a strong association with biological processes such as actin/cytoskeletal associated functions, RNA splicing/turnover, DNA binding/transcription and cell signalling[6]. Notably, variants in actin encoding genes are known to cause human developmental disorders with microcephaly[49-51]. Similarly mandibular

379 and craniofacial features of spliceosomal disorders overlap with patients described here[52].
380 Other possible lines of investigation could also be explored. For example, eIF5A regulates
381 pancreatic cancer metastasis by modulating expression of RhoA and ROCK[53]. Germline
382 variants in several Rho-GTPases cause developmental disorders with microcephaly[54,55].
383 Recently it was shown that hypusinated eIF5A promotes the efficient expression of a subset
384 of mitochondrial proteins involved in the TCA cycle and oxidative phosphorylation[56].
385 Exploring the effects of these mutations on synthesis of mitochondrial proteins and function
386 could be an interesting avenue. Additionally, eIF5A has functions in translation
387 termination[10,11] that we did not explore in this study but which may contribute to this
388 developmental disorder. The importance of eIF5A in neurodevelopment is further
389 emphasised by the recent identification of DHPS deficiency in patients with a
390 neurodevelopmental disorder with seizures and speech and walking impairment (MIM #
391 618480)[57]. The role of eIF5A in normal brain and craniofacial development has never been
392 examined before to the best of our knowledge and the mechanism of how impaired eIF5A
393 results in abnormal neurodevelopment will need to be studied in the future.
394
395 We demonstrated partial rescue of impaired eIF5A function and its resultant phenotypes in
396 yeast and zebrafish models by spermidine (Figs. 3a-c and 4c-d). In yeast, spermidine rescued
397 ribosome association defect and improved the polysome profile and PPT synthesis of the
398 tested mutants. These effects are all consistent with rescuing eIF5A function. However, the
399 molecular mechanism that underlies the rescue remains unclear. As eIF5A expression and
400 hypusination was not increased by spermidine supplement (Fig. 3c), it appears spermidine is
401 not acting via hypusination alone. In agreement with this idea, eIF5A-80S ribosome
402 interaction was enhanced by spermidine (Fig. 3b). How spermidine could boost remaining
403 eIF5A function is not clear. As spermidine rescued transient knockdown of *eif5a* in zebrafish,

it may act similarly to the yeast model, or independently of eIF5A. Of note, our zebrafish model was based on transient knockdown of *eif5a*, and stable germline mutants will need to be studied to resolve these questions in the future. Importantly, spermidine supplementation has been shown to be safe and well tolerated in mice and humans[58]. It promotes longevity in yeast[35] and may extend the lifespan of mice and humans[59,60]. Higher spermidine intake has been shown to be linked to lower mortality in humans[61]. It has also been shown to protect against α-synuclein neurotoxicity in fruit flies[62] and its levels are important for memory-retrieval[63] and age-related memory-associated brain structures in rodents[64]. There is a growing interest in using spermidine as a therapeutic agent in conditions such as cognitive decline[65]. Although the effects of spermidine may be independent of its role in the synthesis of hypusinated-eIF5A, our results raise the interesting possibility of a potential future therapy for individuals with *EIF5A* variant-associated disease.

In summary, we have defined a potentially treatable previously-undescribed human Mendelian disorder caused by *EIF5A* mutations that result in reduced eIF5A-ribosome interactions via mutation-specific mechanisms. The phenotypes are likely explained by impaired synthesis of specific PPT-rich proteins. These findings uncover the role of eIF5A, and proteins with PPTs, in human brain and craniofacial development. Our findings open the avenue for future studies to identify the specific 'hard to synthesise' proteins, and the biological processes, most dependant on eIF5A function.

Methods

Ascertainment and exome sequencing analyses

Seven individuals from seven unrelated families with heterozygous, *de novo*, variants in *EIF5A* were included in this study after informed consents were obtained. The Central Manchester, Cambridge South, and the Republic of Ireland RECs approved this study (02/CM/238, 10/H0305/83 and GEN/284/12, respectively). Informed consent for research studies from patients or their legal representatives was obtained in all cases. The authors affirm that human research participants provided informed consent for publication of the images in Figure 1. The patients were followed up by clinical geneticists from France, the United Kingdom, and the USA. Variants were identified by trio whole-exome sequencing for the detection of an undiagnosed neurodevelopmental disorder associated with multiple congenital anomalies, following published methodology for sample and library preparation, sequencing data production, analysis, and interpretation[66-69]. For the interpretation process we also considered the impact of variants on the preferentially expressed transcript according to the GTEx project[16] and the canonical protein according to UniProtKB[18], and the tolerance of the gene to variation according to gnomAD[19] scores, considering only high quality non-flagged variants present in the "only controls" subset of this database. We considered variants in constrained coding regions only (percentile >90) according to Havrilla, et al.[23]. The clinical observations were gathered through the Matchmaker Exchange[21] and GeneMatcher[22] initiatives.

DNA samples from affected individual 3 and her parents, as well as informed consent, were obtained for PCR and Sanger sequencing confirmation. PCR was performed using primers 5'-AATGGCAGGAGAGGGTGTTT-3' and 5'-TGCAGGTTCAGAGGATCACT-3' and the GoTaq® Hot Start Green Master Mix 2x (PROMEGA). PCR products were purified using an

AxyPrep™ Mag PCR Clean-Up kit (Axygen) and sequenced with a BigDye® Terminator v3.1 Cycle Sequencing kit (Applied Biosystems) on an ABI 3730xl DNA sequencer (Applied Biosystems). The resulting ABI files were examined using the Genome Assembly Program version 4.8b1. Similar Sanger sequencing methods were used to confirm the presence of the *EIF5A* variant in individual 1, and its absence in her parents.

In-silico **analysis of variants and microcephaly-associated genes**

The evolutionary conservation analysis of the residues affected by missense variants was performed using the eIF5A canonical protein sequence from *Homo sapiens* (UniProtKB entry P63241), *Mus musculus* (UniProtKB entry P63242), *Gallus gallus* (UniProtKB entry Q09121), *Danio rerio* (UniProtKB entry Q6NX89, zebrafish hereafter), *Drosophila melanogaster* (UniProtKB entry Q9GU68) and *Saccharomyces cerevisiae* (UniProtKB entry P23301, yeast hereafter) using the ClustalWS alignment in Jalview[70] Version 2. 2.10.5. These residues were modelled in the yeast 60S ribosomal subunit with A-site tRNA, P-site tRNA and eIF5A (PDB entry 5GAK) using Chimera[71] 1.12.

We searched for all genes associated with microcephaly (MAG) deposited in OMIM until 6th February 2018 using the search criteria 'microcephaly (Entries with: gene map locus; Prefixes: +, #; Retrieve: gene map)'. Data were then merged between the OMIM search and the proline content of the human proteome analysed by Morgan and Rubenstein [30] and depicted in Supplementary Table 4.

Gene, variants, morpholinos and plasmid synthesis and expression

A yeast expression plasmid for human eIF5A (*h*eIF5A-WT) was designed to express the human canonical protein sequence, but using the yeast optimised codon usage and placed in the context of the yeast *TIF51A* (*y*eIF5A) 5' and 3' regions. This was commercially synthesised (Epoch Life Sciences) and cloned into a pUC19 vector (Supplementary Note 2), resulting in plasmid pAV2578 (Supplementary Table 1). The gene was subsequently excised using XhoI and SpeI and cloned into SalI-and-SpeI digested single-copy-number (sc) *LEU2* (YCplac111), *URA3* (YCplac33) and high-copy-number (hc) *LEU2* YEplac181 vectors, generating plasmids pAV2580, pAV2592 and pAV2593 (Supplementary Table 1). The *h*eIF5A sequence was verified by Sanger sequencing at Eurofins Genomics using the M13 reverse primer.

The variants p.T48N, p.G106R, p.R109Tfs*8 and p.E122K, detected in individuals 1 to 3 and 7, respectively, were created through site-directed mutagenesis using primers (Supplementary Table 2), the sc pAV2580 plasmid, and the QuikChange Site-Directed Mutagenesis Kit (Agilent Technologies), following the manufacturer's instructions. A hc version of p.R109Tfs*8 was created in pAV2593. The resulting plasmids pAV2584[*h*eIF5A-T48N], pAV2585[*h*eIF5A-G106R], sc pAV2586[*h*eIF5A-R109Tfs*8], pAV2587[*h*eIF5A-E122K] and hc pAV2590[*h*eIF5A-R109Tfs*8 *LEU2*] (Supplementary Table 1) were verified by Sanger sequencing as above.

For genetic knockdown of the *eif5a* gene in zebrafish, an *eif5a* splice site morpholino (MO) was synthesised (Gene Tools, Philomath, OR) for inhibition of the *eif5a* gene (5'-AACCCTATCCAAACATTACCTTTGC-3') as previously published[36]. A standard control MO (5'-CCTCTTACCTCAGTTACAATTTATA-3') by Gene Tools was also used.

Leukocyte transformation and harvesting

Peripheral blood mononuclear cells from one healthy, adult female (Control 1), one healthy, adult male (Control 2), and Individual 3 were transformed by Epstein-Barr virus into lymphoblastoid cell lines (LCLs) following a published protocol[72]. While five million LCLs from Individual 3 were harvested from five cell culture flasks under standard conditions, another five million LCLs from the same individual and number of flasks were treated for 6 hrs with 200 μg/mL of puromycin before harvesting, and both type of samples were kept at -80°C before RNA extraction.

Yeast strain construction and growth assays

The J696 haploid yeast strain deleted for both yeast eIF5A (*ye*IF5A) genes and whose growth is supported by a plasmid bearing *ye*IF5A (Supplementary Table 3), as well as the *ye*IF5A plasmids C3287 (pAV2569), C3288 (pAV2571) and C3294 (pAV2565), and hc PPT reporter plasmids C4351 (pAV2566) and C4353 (pAV2570) (Supplementary Table 1) were kindly provided by Thomas E. Dever, Laboratory of Gene Regulation and Development, National Institute of Child Health and Human Development, National Institutes of Health, Bethesda, USA[2,5].

To study the effect of *h*eIF5A-WT and the variants in yeast, a series of yeast strains was created by transformation and plasmid shuffling of the plasmids described in Supplementary Table 1 into strain J696 to generate the strains described in Supplementary Table 3.

To analyse the effect on yeast growth, *h*eIF5A-WT and its variants, strains GP7439 and GP7443 diploid for *y*eIF5A gene, and hybrid strains, GP7441, GP7447, GP7448, GP7449 and GP7450 containing one *y*eIF5A copy and one *h*eIF5A copy (or *y*eIF5A control) were patched on minimal SD+tryptophan medium, and replica-printed to SD+tryptophan+uracil+5-Fluoro-orotic acid plates to select for loss of the WT *y*eIF5A and create haploid strains GP7440, GP7446, GP7444, GP7455, GP7474 and GP7456 each bearing a different *h*eIF5A or *y*eIF5A plasmid as the sole source of eIF5A. Strains were 10-fold serially diluted and spotted on appropriate selective media ± spermidine at indicated concentrations to record growth phenotypes.

Protein extraction and Western Blotting (WB)

To study the effect of variants on humanised eIF5A synthesis and hypusination, strains GP7444, GP7455, GP7456 and GP7474 were grown in synthetic complete minus leucine (SC-LEU) medium, and strains GP7469, GP7482, GP7484 and GP7485 were grown in synthetic complete minus leucine and uracil (SC-LEU-URA) medium to mid-log phase at 30˚C. To study the effect of variants on synthesis of HA-tagged Ldb17 and Eap1 reporters, all strains between GP7490-GP7493 and between GP7500-GP7503 were grown in SC drop-out medium containing dextrose (0.4%) and galactose (2%) (SCGal-LEU-URA) for 24 hr at 30˚C to induce expression of the PPT reporters. Spermidine (1 mM) was added to media where indicated.

10 OD_{600} units of cells of each strain were harvested, washed and resuspended with 10% trichloroacetic acid, and broken with acid-washed glass beads (Sigma-Aldrich) in a bead-beater (Biospec Products) twice for 45 seconds. These cell extracts were then centrifugated at 20,000 *g* and the pellets resuspended in acetone twice. All these procedures were carried out

544 at 4°C. After a final centrifugation, pellets were dried 10 minutes at 37°C and solubilised in a
545 protease-inhibitor buffer (100 mM Tris-HCl [pH 8.0], 1% SDS, 1 mM EDTA, 1 mM PMSF
546 and 1 cOmplete™ protease inhibitor tablet [Roche]) during 1 hr at 37°C. Then, NuPAGE®
547 LDS Sample Buffer 4X (Invitrogen) and β-mercaptoethanol were added to the extracts,
548 which were subsequently boiled at 95°C during 5 minutes and cooled immediately. After a
549 final spin at 4°C, supernatants were harvested and electrophoresis was carried out using 9-12
550 µL of protein extracts, NuPAGE™ 4-12% Bis-Tris gels (Invitrogen) and NuPAGE™ MOPS
551 SDS 20X running buffer (Invitrogen) during 50 minutes at 200V. The Precision Plus
552 Protein™ All Blue Prestained Protein Standard (Bio-Rad Laboratories Ltd., UK) was used as
553 molecular weight marker. Gels were blotted onto Amersham™ Protan™ 0.45 µm
554 nitrocellulose membranes (General Electric Healthcare), and using Whatman™ 3 mm Chr
555 chromatography paper (General Electric Healthcare), NuPAGE™ 20X transfer buffer
556 (Invitrogen), and XCell™ Blot module (Invitrogen) during 1 h at 30 V. After blocking non-
557 specific binding, the membranes were incubated overnight at 4°C with specific mouse anti-
558 eIF5A (1:10,000; BD Biosciences, #611977), rabbit anti-hypusine (1:1,000; EMD Millipore,
559 #ABS1064), mouse anti-Pab1 (1:5,000; EnCor Biotechnology, #MCA-1G1), mouse anti-
560 HA.11 (1:4,000; BioLegend, #901513) or chicken anti-eIF2α (1:500; Cambridge Research
561 Biochemicals, custom designed). Then, the membranes were incubated with a corresponding
562 secondary fluorescent labelled donkey anti-chicken (P/N: 926-32218), and goat anti-rabbit
563 (P/N: 926-32211) or anti-mouse antibodies (P/N: 926-32350) (IRDye® 800CW, LI-COR
564 Biosciences) and the signal was developed using a LI-COR Odyssey® CLx Imaging System
565 (LI-COR Biosciences) using default parameters. The area of every band was selected to fit it
566 to the best curve of fluorescence.
567

The precise epitope recognised by the commercial eIF5A monoclonal antibody is not known. It was raised to a protein 58-154 and our work shows it cross-reacts with the R109Tfs*8 mutant (Supplementary Figure 4), implying its epitope is between 58 and 108. As the antibody cross-reacts with all mutant forms tested here we assume that G106 is not part of its binding site on eIF5A. Pab1 encoding the yeast polyA binding protein was used as a loading control for most assays. However, Ldb17 with HA tag and Pab1 co-migrate in SDS-PAGE gels and some residual fluorescence remained for both proteins after stripping. Therefore, eIF2α antibodies were used as a loading control for blots for experiments using Ldb17-HA expressing strains. Full scans of representative western blots shown in Fig 2b, 2d and 3c are depicted in Supplementary Figures 9, 11 and 13.

Polysome profile analysis

The GP7444, GP7455, GP7456 and GP7474 strains were grown to mid-log phase at 30˚C in 80 ml of SC-LEU medium ± spermidine (1 mM). 50 mM of formaldehyde was added followed immediately by 15 ml of pre-made frozen media droplets. We used formaldehyde treatment to stabilize polysomes and bound factors rather than cycloheximide, because the latter has been found to enhance eIF5A-ribosome interactions[24]. Cross-linking was then carried out on ice water for 1 hr before quenching with glycine (final concentration of 100 mM). Whole cell extracts were prepared by bead beating in lysis buffer (20 mM hepes, 2 mM magnesium acetate, 100 mM potassium acetate, 0.5 mM DTT), clarified (10,000 x g 10 min) and separated on 15-50% sucrose gradients by centrifugation at 40,000 rpm for 2.5 h using a SW41 Beckman rotor. Gradients were fractionated while scanning at A_{254} to visualize the indicated ribosomal species. Polysome to monosome (P/M) and 60S/80S ratios were calculated by comparing the areas under the 60S, 80S and polysome peaks. Gradient fractions were TCA precipitated and underwent western blot analysis using antibodies as described

above as well as Rps3(uS3) (1:50,000) and Rpl35(uL29) (1:10,000) rabbit polyclonal antibodies (a kind gift from Dr Martin Pool, University of Manchester). Full scans of representative western blots shown in Fig. 2c and 3b are depicted in Supplementary Figures 10 and 12, respectively.

RNA extraction and quantitative real-time PCR (qRT-PCT)

Total RNA was extracted using RNeasy Mini kit (Qiagen) according to the manufacturer's protocol from 1 million LCLs of Control 1 and Control 2 each, and from 1 million, untreated LCLs and 1 million puromycin-treated LCLs of Individual 3. RNA concentration was measured using a NanoDrop 2000 spectrophotometer (Thermo Scientific). RNA was reverse transcribed with random hexamer primers (Promega) to generate cDNA using the M-MLV Reverse Transcriptase kit (Promega) according to the manufacturer's protocol. qRT-PCR reactions were performed on a Bio-Rad CFX394 Real Time system (Bio-Rad) using Power SYBR Green PCR Master mix (Applied Biosystems) and the forward 5'-GCCATGTAAGATCGTCGAGA-3' and reverse 5'-GGAGCAGTGATAGGTACCCA-3' *EIF5A* primers (Sigma-Aldrich). The level of *EIF5A* mRNA was evaluated using a relative quantification approach (2-ΔCT method) with human *GAPDH* and its primers 5'-ATGGGGAAGGTGAAGGTCG -3'and 5'-TAAAAGCAGCCCTGGTGACC-3' as the internal reference. To detect if the frameshift-encoding transcript is expressed, we performed bidirectional Sanger sequencing of Individual 3's *EIF5A* cDNA, obtained from both untreated and puromycin-treated LCLs, using the aforementioned forward primer and reverse 5'-GCCTTGATTGCAACAGCTGC-3' primer, as previously described.

Zebrafish knockdown, staining and imaging

Zebrafish husbandry was approved by The University of Manchester Ethical Review Board and all experiments were performed in accordance with UK Home Office regulations (PPL P132EB6D7). Four hundred pg (in 1 nL) of either the *eif5a* or control MOs were injected into 25-75 fertilised nacre embryos per condition, at the single cell stage. Injected embryos were incubated at 28°C in standard E3 embryo medium (SE3EM) until 3hpf and then split into two groups, one of them only in SE3EM and the other one in SE3EM plus Spermidine (85558, Sigma-Aldrich) to a final concentration of 1 µM. Both groups were incubated at 28°C until 77 hpf, without renewing the media.

At 77 hpf, larvae were terminated using 4% MS222 and fixed for 1 hour with 2% paraformaldehyde, and then stained using a two-color acid-free bone and cartilage staining protocol[73]. Stained larvae groups were blinded to manipulator, mounted into 4% methylcellulose and imaged using a DFC7000 T Camera (Leica) coupled to a M165 FC Microscope (Leica) using 10x objective and LASX image capture software (version 3.4.2; Leica). Head size and mandibles were measured as depicted in Fig. 4a using ImageJ software (version 1.52j).

Statistics

All statistics were calculated with either GraphPad Prism 8.3.0 (GraphPad Software) or SPSS v25 (IBM) and all experiments were carried out using three biological (yeast and zebrafish analyses) or technical (Individual 3's *EIF5A* RNA expression) replicates. Chi-square was performed to study the association between content of PPTs and MAGs. Signals of WBs from yeast extracts were normalised to the mean signal across each blot for each antibody and for loading variance between lanes using similarly normalised control antibody signals as

follows in Equation (1): $ab\ ratio = \frac{\frac{Tab}{Mean\ Tab}}{\frac{Cab}{Mean\ Cab}} = \frac{Tab \times Mean\ Cab}{Mean\ Tab \times Cab}$, where Tab is the Test antibody and Cab the Control antibody. For hypusine quantification, eIF5A was used as its control antibody. Unpaired t-test against control samples was performed for western blots from yeast extracts and for Individual 3 *EIF5A* RNA expression. These results were depicted using bar plots, which represent the mean (average) plus standard error of the mean with overlaid data points representing independent experiments. Kruskal Wallis test with multiple comparisons was performed for zebrafish analyses. These results were depicted using dot plots and the longer horizontal line represents the median, whereas the shorter horizontal lines are the 25th and 75th percentiles. A p-value below 0.05 was considered significant, which is given at the top of each graph, where relevant.

Data availability

List of public databases and programmes used, serial dilutions depicted in Fig 2a and 3a and Supplementary Figs. 3 and 8, and zebrafish morpholino work is deposited in "Source Data" zip file. Full data of poly-proline tracts in microcephaly-associated genes is depicted in Supplementary Table 4. Full uncropped scans of representative western blots shown in Figs. 2b, 2c, 2d, 3b, 3c, and Supplementary Figs. 4, 6 and 7 are depicted in the "Supplementary Information" file.

References

1. Melnikov, S. *et al.* Molecular insights into protein synthesis with proline residues. *EMBO Rep* **17**, 1776-1784 (2016).

2. Saini, P., Eyler, D.E., Green, R. & Dever, T.E. Hypusine-containing protein eIF5A promotes translation elongation. *Nature* **459**, 118-21 (2009).
3. Nishimura, K., Lee, S.B., Park, J.H. & Park, M.H. Essential role of eIF5A-1 and deoxyhypusine synthase in mouse embryonic development. *Amino Acids* **42**, 703-10 (2012).
4. Turpaev, K.T. Translation Factor eIF5A, Modification with Hypusine and Role in Regulation of Gene Expression. eIF5A as a Target for Pharmacological Interventions. *Biochemistry (Mosc)* **83**, 863-873 (2018).
5. Gutierrez, E. *et al.* eIF5A promotes translation of polyproline motifs. *Mol Cell* **51**, 35-45 (2013).
6. Jan, E., Mandal, A., Mandal, S. & Park, M.H. Genome-Wide Analyses and Functional Classification of Proline Repeat-Rich Proteins: Potential Role of eIF5A in Eukaryotic Evolution. *PLoS ONE* **9**, e111800 (2014).
7. Park, M.H., Nishimura, K., Zanelli, C.F. & Valentini, S.R. Functional significance of eIF5A and its hypusine modification in eukaryotes. *Amino Acids* **38**, 491-500 (2010).
8. Ivanov, I.P. *et al.* Polyamine Control of Translation Elongation Regulates Start Site Selection on Antizyme Inhibitor mRNA via Ribosome Queuing. *Mol Cell* **70**, 254-264 e6 (2018).
9. Manjunath, H. *et al.* Suppression of Ribosomal Pausing by eIF5A Is Necessary to Maintain the Fidelity of Start Codon Selection. *Cell Reports* **29**, 3134-3146.e6 (2019).
10. Schuller, A.P., Wu, C.C.-C., Dever, T.E., Buskirk, A.R. & Green, R. eIF5A Functions Globally in Translation Elongation and Termination. *Molecular Cell* **66**, 194-205.e5 (2017).

11. Pelechano, V. & Alepuz, P. eIF5A facilitates translation termination globally and promotes the elongation of many non polyproline-specific tripeptide sequences. *Nucleic Acids Research* **45**, 7326-7338 (2017).
12. Hoque, M. *et al.* Regulation of gene expression by translation factor eIF5A: Hypusine-modified eIF5A enhances nonsense-mediated mRNA decay in human cells. *Translation (Austin)* **5**, e1366294 (2017).
13. Mathews, M.B. & Hershey, J.W. The translation factor eIF5A and human cancer. *Biochim Biophys Acta* **1849**, 836-44 (2015).
14. Wang, Z., Jiang, J., Qin, T., Xiao, Y. & Han, L. EIF5A regulates proliferation and chemoresistance in pancreatic cancer through the sHH signalling pathway. *Journal of Cellular and Molecular Medicine* **23**, 2678-2688 (2019).
15. Banka, S. *et al.* How genetically heterogeneous is Kabuki syndrome?: MLL2 testing in 116 patients, review and analyses of mutation and phenotypic spectrum. *Eur J Hum Genet* **20**, 381-8 (2012).
16. GTEx Consortium. Human genomics. The Genotype-Tissue Expression (GTEx) pilot analysis: multitissue gene regulation in humans. *Science* **348**, 648-60 (2015).
17. Cunningham, F. *et al.* Ensembl 2019. *Nucleic Acids Res* **47**, D745-D751 (2019).
18. Breuza, L. *et al.* The UniProtKB guide to the human proteome. *Database (Oxford)* **2016**(2016).
19. Karczewski, K.J. *et al.* The mutational constraint spectrum quantified from variation in 141,456 humans. *Nature* **581**, 434-443 (2020).
20. Abramovs, N., Brass, A. & Tassabehji, M. GeVIR is a continuous gene-level metric that uses variant distribution patterns to prioritize disease candidate genes. *Nature Genetics* **52**, 35-39 (2019).

21. Philippakis, A.A. *et al.* The Matchmaker Exchange: a platform for rare disease gene discovery. *Hum Mutat* **36**, 915-21 (2015).
22. Sobreira, N., Schiettecatte, F., Valle, D. & Hamosh, A. GeneMatcher: a matching tool for connecting investigators with an interest in the same gene. *Hum Mutat* **36**, 928-30 (2015).
23. Havrilla, J.M., Pedersen, B.S., Layer, R.M. & Quinlan, A.R. A map of constrained coding regions in the human genome. *Nat Genet* **51**, 88-95 (2019).
24. Schmidt, C. *et al.* Structure of the hypusinylated eukaryotic translation factor eIF-5A bound to the ribosome. *Nucleic Acids Res* **44**, 1944-51 (2016).
25. de Goede, C. *et al.* Role of reverse phenotyping in interpretation of next generation sequencing data and a review of INPP5E related disorders. *Eur J Paediatr Neurol* **20**, 286-95 (2016).
26. Mastracci, T.L., Robertson, M.A., Mirmira, R.G. & Anderson, R.M. Polyamine biosynthesis is critical for growth and differentiation of the pancreas. *Sci Rep* **5**, 13269 (2015).
27. Parreiras-e-Silva, L.T. *et al.* Evidences of a role for eukaryotic translation initiation factor 5A (eIF5A) in mouse embryogenesis and cell differentiation. *J Cell Physiol* **225**, 500-5 (2010).
28. Cano, V.S. *et al.* Mutational analyses of human eIF5A-1--identification of amino acid residues critical for eIF5A activity and hypusine modification. *FEBS J* **275**, 44-58 (2008).
29. Amberger, J.S., Bocchini, C.A., Schiettecatte, F., Scott, A.F. & Hamosh, A. OMIM.org: Online Mendelian Inheritance in Man (OMIM(R)), an online catalog of human genes and genetic disorders. *Nucleic Acids Res* **43**, D789-98 (2015).

30. Morgan, A.A. & Rubenstein, E. Proline: the distribution, frequency, positioning, and common functional roles of proline and polyproline sequences in the human proteome. *PLoS One* **8**, e53785 (2013).
31. Ng, S.B. *et al.* Exome sequencing identifies MLL2 mutations as a cause of Kabuki syndrome. *Nat Genet* **42**, 790-3 (2010).
32. Bernier, F.P. *et al.* Haploinsufficiency of SF3B4, a component of the pre-mRNA spliceosomal complex, causes Nager syndrome. *Am J Hum Genet* **90**, 925-33 (2012).
33. Shin, B.S. *et al.* Amino acid substrates impose polyamine, eIF5A, or hypusine requirement for peptide synthesis. *Nucleic Acids Res* **45**, 8392-8402 (2017).
34. Chattopadhyay, M.K., Tabor, C.W. & Tabor, H. Spermidine but not spermine is essential for hypusine biosynthesis and growth in Saccharomyces cerevisiae: spermine is converted to spermidine in vivo by the FMS1-amine oxidase. *Proc Natl Acad Sci U S A* **100**, 13869-74 (2003).
35. Eisenberg, T. *et al.* Induction of autophagy by spermidine promotes longevity. *Nat Cell Biol* **11**, 1305-14 (2009).
36. Carvalho, C.M. *et al.* Dosage changes of a segment at 17p13.1 lead to intellectual disability and microcephaly as a result of complex genetic interaction of multiple genes. *Am J Hum Genet* **95**, 565-78 (2014).
37. White, R.M. *et al.* Transparent adult zebrafish as a tool for in vivo transplantation analysis. *Cell Stem Cell* **2**, 183-9 (2008).
38. Cooper, D.N., Mort, M., Stenson, P.D., Ball, E.V. & Chuzhanova, N.A. Methylation-mediated deamination of 5-methylcytosine appears to give rise to mutations causing human inherited disease in CpNpG trinucleotides, as well as in CpG dinucleotides. *Human Genomics* **4**, 406 (2010).

39. Pällmann, N. *et al.* Biological Relevance and Therapeutic Potential of the Hypusine Modification System. *Journal of Biological Chemistry* **290**, 18343-18360 (2015).
40. Leegwater, P.A. *et al.* Subunits of the translation initiation factor eIF2B are mutant in leukoencephalopathy with vanishing white matter. *Nat Genet* **29**, 383-8 (2001).
41. Borck, G. *et al.* eIF2gamma mutation that disrupts eIF2 complex integrity links intellectual disability to impaired translation initiation. *Mol Cell* **48**, 641-6 (2012).
42. Martin, H.C. *et al.* Quantifying the contribution of recessive coding variation to developmental disorders. *Science* **362**, 1161-1164 (2018).
43. Gkogkas, C.G. *et al.* Autism-related deficits via dysregulated eIF4E-dependent translational control. *Nature* **493**, 371-7 (2013).
44. Neves-Pereira, M. *et al.* Deregulation of EIF4E: a novel mechanism for autism. *J Med Genet* **46**, 759-65 (2009).
45. Santini, E. *et al.* Exaggerated translation causes synaptic and behavioural aberrations associated with autism. *Nature* **493**, 411-5 (2013).
46. Chartier-Harlin, M.C. *et al.* Translation initiator EIF4G1 mutations in familial Parkinson disease. *Am J Hum Genet* **89**, 398-406 (2011).
47. Zeesman, S. *et al.* Microdeletion in distal 17p13.1: A recognizable phenotype with microcephaly, distinctive facial features, and intellectual disability. *American Journal of Medical Genetics Part A* **158A**, 1832-1836 (2012).
48. Umland, T.C., Wolff, E.C., Park, M.H. & Davies, D.R. A New Crystal Structure of Deoxyhypusine Synthase Reveals the Configuration of the Active Enzyme and of an Enzyme·NAD·Inhibitor Ternary Complex. *Journal of Biological Chemistry* **279**, 28697-28705 (2004).
49. Riviere, J.B. *et al.* De novo mutations in the actin genes ACTB and ACTG1 cause Baraitser-Winter syndrome. *Nat Genet* **44**, 440-4, S1-2 (2012).

50. Cuvertino, S. *et al.* ACTB Loss-of-Function Mutations Result in a Pleiotropic Developmental Disorder. *Am J Hum Genet* **101**, 1021-1033 (2017).
51. Latham, S.L. *et al.* Variants in exons 5 and 6 of ACTB cause syndromic thrombocytopenia. *Nature Communications* **9**(2018).
52. Lehalle, D. *et al.* A review of craniofacial disorders caused by spliceosomal defects. *Clinical Genetics* **88**, 405-415 (2015).
53. Fujimura, K. *et al.* Eukaryotic Translation Initiation Factor 5A (EIF5A) Regulates Pancreatic Cancer Metastasis by Modulating RhoA and Rho-associated Kinase (ROCK) Protein Expression Levels. *J Biol Chem* **290**, 29907-19 (2015).
54. Reijnders, M.R.F. *et al.* RAC1 Missense Mutations in Developmental Disorders with Diverse Phenotypes. *Am J Hum Genet* **101**, 466-477 (2017).
55. Zamboni, V. *et al.* Rho GTPases in Intellectual Disability: From Genetics to Therapeutic Opportunities. *Int J Mol Sci* **19**(2018).
56. Puleston, D.J. *et al.* Polyamines and eIF5A Hypusination Modulate Mitochondrial Respiration and Macrophage Activation. *Cell Metabolism* **30**, 352-363.e8 (2019).
57. Ganapathi, M. *et al.* Recessive Rare Variants in Deoxyhypusine Synthase, an Enzyme Involved in the Synthesis of Hypusine, Are Associated with a Neurodevelopmental Disorder. *Am J Hum Genet* **104**, 287-298 (2019).
58. Schwarz, C. *et al.* Safety and tolerability of spermidine supplementation in mice and older adults with subjective cognitive decline. *Aging (Albany NY)* **10**, 19-33 (2018).
59. Eisenberg, T. *et al.* Cardioprotection and lifespan extension by the natural polyamine spermidine. *Nat Med* **22**, 1428-1438 (2016).
60. Madeo, F., Eisenberg, T., Pietrocola, F. & Kroemer, G. Spermidine in health and disease. *Science* **359**, eaan2788 (2018).

61. Kiechl, S. *et al.* Higher spermidine intake is linked to lower mortality: a prospective population-based study. *Am J Clin Nutr* **108**, 371-380 (2018).
62. Buttner, S. *et al.* Spermidine protects against alpha-synuclein neurotoxicity. *Cell Cycle* **13**, 3903-8 (2014).
63. Tiboldi, A. *et al.* Hippocampal polyamine levels and transglutaminase activity are paralleling spatial memory retrieval in the C57BL/6J mouse. *Hippocampus* **22**, 1068-74 (2012).
64. Liu, P., Gupta, N., Jing, Y. & Zhang, H. Age-related changes in polyamines in memory-associated brain structures in rats. *Neuroscience* **155**, 789-96 (2008).
65. Wirth, M. *et al.* Effects of spermidine supplementation on cognition and biomarkers in older adults with subjective cognitive decline (SmartAge)—study protocol for a randomized controlled trial. *Alzheimer's Research & Therapy* **11**(2019).
66. Deciphering Developmental Disorders Study. Prevalence and architecture of de novo mutations in developmental disorders. *Nature* (2017).
67. Faundes, V. *et al.* Histone Lysine Methylases and Demethylases in the Landscape of Human Developmental Disorders. *Am J Hum Genet* **102**, 175-187 (2018).
68. Retterer, K. *et al.* Clinical application of whole-exome sequencing across clinical indications. *Genet Med* **18**, 696-704 (2016).
69. Gordon, Christopher T. *et al.* Mutations in Endothelin 1 Cause Recessive Auriculocondylar Syndrome and Dominant Isolated Question-Mark Ears. *The American Journal of Human Genetics* **93**, 1118-1125 (2013).
70. Waterhouse, A.M., Procter, J.B., Martin, D.M., Clamp, M. & Barton, G.J. Jalview Version 2--a multiple sequence alignment editor and analysis workbench. *Bioinformatics* **25**, 1189-91 (2009).

71. Pettersen, E.F. *et al.* UCSF Chimera--a visualization system for exploratory research and analysis. *J Comput Chem* **25**, 1605-12 (2004).

72. Frisan, T., Levitsky, V. & Masucci, M. Generation of Lymphoblastoid Cell Lines (LCLs). in *Epstein-Barr Virus Protocols* (eds. Wilson, J.B. & May, G.H.W.) 125-127 (Humana Press, Totowa, NJ, 2001).

73. Walker, M.B. & Kimmel, C.B. A two-color acid-free cartilage and bone stain for zebrafish larvae. *Biotech Histochem* **82**, 23-8 (2007).

Acknowledgements

We are thankful to all the individuals and their families for taking part in the study. We thank Tom Dever (National Institutes of Health, USA) and Beth Grayhack (University of Rochester Medical Center, USA) for kind gifts of plasmids and yeast strains used in this study, as well as Martin Pool (University of Manchester, UK) for the gift of antibodies to ribosomal proteins.

We are thankful to the Deciphering Developmental Disorders (DDD) study for the invaluable collaboration. The DDD Study (Cambridge South REC approval 10/H0305/83 and the Republic of Ireland REC GEN/284/12) presents independent research commissioned by the Health Innovation Challenge Fund (grant number HICF-1009-003), a parallel funding partnership between the Wellcome Trust and the Department of Health, and the Wellcome Trust Sanger Institute (grant number WT098051). The views expressed in this publication are those of the author(s) and not necessarily those of the Wellcome Trust, BBSRC or the Department of Health. The research team acknowledges the support of the National Institute for Health Research, through the Comprehensive Clinical Research Network, UK.

V.F. acknowledges to CONICYT, Chile's National Commission for Scientific and Technological Research, for its scholarship support (grant number 72160007). V.F., W.G.N. and S.B. acknowledge to the Kabuki Research Fund at Manchester University NHS Foundation Trust. W.G.N. acknowledges support from Action Medical Research (GN2494), and the Manchester NIHR Biomedical Research Centre (IS-BRC-1215-20007). G.D.P. and M.D.J. acknowledge to Biotechnology and Biological Sciences Research Council (BBSRC), UK, for its financial support (grant BB/N014049/1). P.R.K and S.Cr were supported by the Stroke Association (TSA LECT 2017/02) and the NC3Rs (NC/N002598/1).J.A. and C.T.G. were supported by the Agence Nationale de la Recherche (CranioRespiro project and

862 “Investissements d’avenir” program (ANR-10-IAHU-01)) and MSDAvenir (DevoDecode
863 project).
864

865 Author contributions

866 S.B. conceived the project. S.B., G.D.P., P.R.K, W.G.N., V.F. and M.D.J. designed the study.
867 S.J.D., A.D., A.F., V.H., J.A., D.L., P.N., J.R., M.S., L.C., C.J.S., B.R.S., J.L.G. and C.T.G
868 provided patients’ phenotypes and collected samples. V.F. performed compilation of patients’
869 clinical data, *in-silico* analysis of variants, association of PPT with MAGs, Sanger
870 sequencing confirmation, synthesis of gene, variants and yeast plasmids, cell transformations,
871 yeast growth assays and western blots. M.D.J. performed polysome fractionation and western
872 blot analysis. S.L, S.Cr. and S.E.W. performed zebrafish injections, staining and imaging.
873 S.Cu. performed RNA extraction, expression analysis and sequencing of cDNA, and western
874 blot of human samples. V.F., S.B., G.D.P., P.R.K. and M.D.J. wrote the manuscript. All
875 authors reviewed, edited, and approved the final manuscript.
876

877 Competing interests

878 The authors declare no competing interests.

Figure legends

Figure 1. Heterozygous variants in *EIF5A* cause a novel craniofacial-neurodevelopmental disorder.

a) Individuals with *de novo* heterozygous missense (individuals 1, 2, 4 and 7) or frameshift (individual 3) *EIF5A* variants display similar facial dysmorphism, microcephaly and micrognathia. Photographs of individuals 5 and 6 are not available. **b**) The missense *EIF5A* variants affect highly conserved residues. Evolutionary conservation of residues affected by variants (delimited by yellow rectangles), is shown in five species. BLOSUM62 scores are depicted in purple scale (dark purple=completely conserved, light purple= relatively conserved, white=not conserved). Lysine (K) 50 is hypusinated (Hyp). **c**) The *EIF5A* variants are novel and located in the functional sites and domains of eIF5A. Top: hypusine site (HS) is the orange bar between residues 48 and 55 (InterPro entry P63241), and the OB fold domain is the cyan bar between residues 83 and 150 (InterPro entry P63241). Bottom: the location and the minor allele frequencies (MAF) of high quality non-flagged missense variants (yellow triangles) and a protein-truncating variant (p.N28Mfs*64, magenta line) seen only in controls of gnomAD v2.1.1 for the transcript ENST00000336458. **d**) *In-silico* modelling of missense variants supports their deleterious nature. Variants are indicated as red spheres at the surface of yeast eIF5A (semi-transparent gold) with hypusinated K51 (human K50, *h*K50) (black spheres) shown bound to the yeast 60S ribosomal subunit E site (grey secondary structures only, with uL1 in blue), with adjacent P-site (green) and A-site (pink) tRNAs (PDB entry 5gak). Note that T48 (yeast T49, *y*T49) is in proximity to the hypusinated *h*K50; *h*G106 (yG107) and *h*R109 (*y*K110*)* are close to uL1 and *h*E122 (*y*S123) is close to the P-site tRNA. **e**) The mutant *EIF5A* transcript with the truncating variant is not expressed. The mRNA levels in lymphoblastoid cells from individual 3 compared to control 1 (healthy female) and control 2 (healthy male) are shown relative to *GAPDH* ($2^{-\Delta CT}$ method). Each data point

corresponds to one technical replicates, and the bars show the mean + s.e.m. Two-sided *P* values were determined by un-paired t-test.

Figure 2. *EIF5A* variants impair eIF5A function, its interaction with ribosome and synthesis of proteins with poly-proline tracts.

a) Variants p.T48N and p.G106R affect yeast growth. Representative serial dilution growth assay of yeast strains for human eIF5A (*h*eIF5A) and its variants, compared to the growth of strains with WT yeast eIF5A (*y*eIF5A) or the thermosensitive *y*eIF5A-S149P after two days. Eighteen replicates per temperature were performed. **b**) Variant p.T48N reduces eIF5A hypusination, whereas p.G106R and p.E122K decrease eIF5A levels. eIF5A expression (left) and hypusination (Hyp; right) amongst yeast strains with missense *h*eIF5A variants, grown at 30°C in synthetic complete (SC) liquid medium. Each data point corresponds to one biological replicate, which was controlled as stated in the methods (see Equation (1)), and the bars show the mean + s.e.m. Two-sided *P* values were determined by un-paired t-test. Full uncropped images of gel blots are shown in Supplementary Figure 9. **c**) Missense mutants decrease eIF5A interaction with ribosome. Polysome profiles of yeast expressing either *h*eIF5A-WT or missense variants, grown at 30°C in SC medium. Corresponding western blot analyses of eIF5A, hypusine, and the ribosomal proteins uS3 and uL29 probed across gradient fractions for each polysome profile are presented beneath. Polysome to monosome (P/M) and 60/80S ratios for the A_{260} traces are given, calculated by comparing the areas under the 80S and polysome peaks. In addition, the fraction of total eIF5A signal associated with the 80S (western blot lane 6) is given. Full uncropped images of gel blots are shown in Supplementary Figure 10. One profile was performed. **d**) Missense mutants decrease synthesis of reporters with poly-proline tracts. Comparison of Ldb17 (left graph) and Eap1 (right graph) poly-proline-containing reporter expression in *h*eIF5A yeast strains grown at

30°C in SCGal medium. Data presentation and statistical treatment as described for panel **b**. Full uncropped images of gel blots are shown in Supplementary Figure 11. **e**) Genes with the highest numbers of prolines match the initial clinical suspicion for studied individuals. Enrichment of PPTs in MAGs. For each MAG the number of PPTs (X axis) is plotted against the number of prolines in the longest PPT (Y axis). MAG circle size represents the total number of prolines in PPTs in each protein. The 'top 10' ranked MAGs are named. Heterozygous loss-of-function variants in *SF3B4* and *KMT2D* (both underlined) cause acrofacial dysostosis 1, Nager type (a subtype of mandibulofacial dysostosis, MIM #154400) and Kabuki syndrome 1 (MIM #147920), respectively, which overlap with the initial clinical suspicions in individual 1, and for individuals 2 to 4, respectively.

Figure 3. Spermidine partially rescues impaired eIF5A function phenotypes in yeast.

a) Spermidine rescues growth of p.T48N and p.G106R strains. Growth of yeast strains for the human eIF5A (*h*eIF5A) and the missense variants in minimum media supplemented with 0 mM (Untreated), 1 mM and 2 mM of spermidine at 30°C. Eighteen replicates per temperature were performed. **b**) Spermidine increases the interaction of *h*eIF5A-T48N and *h*eIF5A-G106R with ribosomes. Polysome profiles of *h*eIF5A-WT, *h*eIF5A-T48N and *h*eIF5A-G106R grown at 30°C in SC with 1 mM spermidine. Corresponding western blot analyses as described in the legend to Figure 2c. Full uncropped images of gel blots are shown in Supplementary Figure 12. One profile was performed. **c**) Spermidine increases the synthesis of Ldb17 reporter in both p.T48N and p.G106R strains. Comparison of Ldb17 (left graph), total eIF5A (middle graph) and hypusinated eIF5A (right graph) amongst *h*eIF5A yeast strains, grown at 30°C in SCGal with and without 1 mM spermidine. Data presentation and statistics as described in the legend to Fig. 2b. Full uncropped images of gel blots are shown in Supplementary Figure 13.

Figure 4. Knockdown of *eif5a* in zebrafish embryos induces micrognathia, which can be partially rescued by spermidine.

a) Measurement of iris distance was used for assessing head size (left photograph), and both Meckel's (M) plus both palatoquadrate (Pq) cartilages for mandible assessment (right photograph). **b**) Spermidine partially rescues micrognathia. Representative images of alcian blue stained zebrafish larvae injected with 400 pg (1 nL) of either control or *eif5a* MOs. Larvae were incubated at 28°C for 3 hours in standard E3 embryo medium (SE3EM) and then transferred to either fresh SE3EM or fresh SE3EM plus 1 μM spermidine at 28°C, and processed after 77 hours post-fertilisation. **c**) Quantification of measurements shown in panel **a**. Each data point corresponds to one fish, the longer horizontal line represents the median, whereas the shorter horizontal lines are the 25^{th} and 75^{th} percentiles. P values were determined by Kruskal Wallis test with multiple comparisons. *P*-values for comparisons against control MO injected fish are provided when less than 0.05.

Tables

Table 1. Phenotypes of patients with *EIF5A* variants.

Characteristics	Individual						
	1	2	3	4	5	6	7
Sex (age)[a]	F (6.9 y)	F (8.4 y)	F (8.4y)	M (18.3y)	M (8 mo)	M (4 y)	F (16.4y)
Genomic position[b]	17:7213097	17:7214714	17:7214722	17:7214723	17:7214723	17:7214741	17:7214762
cDNA[c] **protein consequence**[d]	c.143C>A p.T48N	c.316G>A p.G106R	c.324dupA p.R109Tfs*8	c.325C>G p.R109G	c.325C>T p.R109*	c.343C>T p.P115S	c.364G>A p.E122K
Inheritance/ zygosity	DN Het	DN Het	DN Het	DN Het	DN Het	DN Het	DN Het
Perinatal history							
Congenital microcephaly	Yes	Yes	Yes	Unknown	No	No	Unknown
IUGR	Yes	Yes	No	Yes	No	No	No
Feeding difficulties	No	Yes	Yes	Yes	Yes	No	No
Other	No	Cardiac anomalies	Cardiac anomalies Cleft palate	Hypotonia	Cardiac anomalies Hypotonia	No	Foetal ascites
DD/ID	Moderate/ severe	Moderate	Mild	Moderate	Moderate	Mild/Moderate	Moderate
CNS anomalies	No	No	No	Peritrigonal hyperintensities	No	Left lateral ventriculomegaly	No
Physical anomalies							
Heart	No	Yes	Yes	Unknown	Yes	Unknown	Unknown
Craniofacial	Yes	No	Yes	Yes	Yes	No	No
Other	Hemivertebrae (L3)	No	No	Cryptorchidism Pes planus	No	No	Toe contractures Small toenails Pes planus
Growth Parameters							
Height (SD)	N (0.53)	SS (-2.82)	N (0.86)	N (-0.45)	N (-1.45)	N (+1 SD),	SS (-2.59)
Weight (SD)	O (2)	LW (-2.28)	N (-0.41)	N (0.06)	LW (-3.14)	N (-0.09 SD)	N (-0.69)
HC (SD)	Mi (-3)	Mi (-7.47)	Mi (-2.11)	Mi (-2.62)	N (-0.45)	N (-1.09)	Mi (-1.94)
Facial dysmorphisms							
- Broad eyebrows	Yes	Yes	Yes	Yes	No	Yes	No
- Abn. supraorbital ridges	Yes	Yes	Yes	Yes	No	No	No
- Epi/telecanthus	No	Yes	Yes	Yes	Yes	No	Yes
- Bulbous nasal tip	Yes	Yes	Yes	Yes	No	No	No
- Thin upper lip	No	Yes	Yes	Yes	Yes	No	No
- Micrognathia	Yes	Yes	Yes	Yes	No	Yes	No
- Low set ears	Yes	Yes	No	No	No	No	Yes
- Other	Lower eyelid hypoplasia	Hypertelorism	No	Prominent long ears	Plagiocephaly Sparse scalp hair Frontal bossing Downslanting PF Cupped ears	Long PF hypoplastic ala nasi	Deep-set eyes Abn. lower eyelids Small ears

Other medical issues							
Joint hypermobility	No	No	Yes	Yes	N/A	No	Yes
Eye anomalies	Yes	No	No	Yes	No	Yes	Yes
Other	No	Constipation Gastroesophageal reflux Gastrostomy	Conductive deafness Premature thelarche	Constipation	Dysphagia Gastrostomy Failure to thrive	Hypotonia Flat feet	Autism ADHD Delayed puberty Nasal polyps
Initial clinical suspicion	Mandibulofacial dysostosis	Kabuki syndrome like	Kabuki syndrome like	Kabuki syndrome like	Mowat Wilson	None	None

[a] At last examination; [b] According to hg19; [c] GenBank reference NM_001970.5, Ensembl reference ENST00000336458; [d] UniProtKB reference P63241-1

Abbreviations: Abn=abnormal, ADHD=attention deficit hyperactivity disorder; CNS=Central nervous system, DD= Developmental delay, HC=Head circumference, Het=Heterozygous, ID=Intellectual disability, IUGR=Intra-uterine growth retardation, LW=Low weight, Mi=Microcephaly, N=Within normal ranges, N/A=Not applicable, O=Obesity, PF=Palpebral fissures, SD=Standard deviation, SS=Short stature.

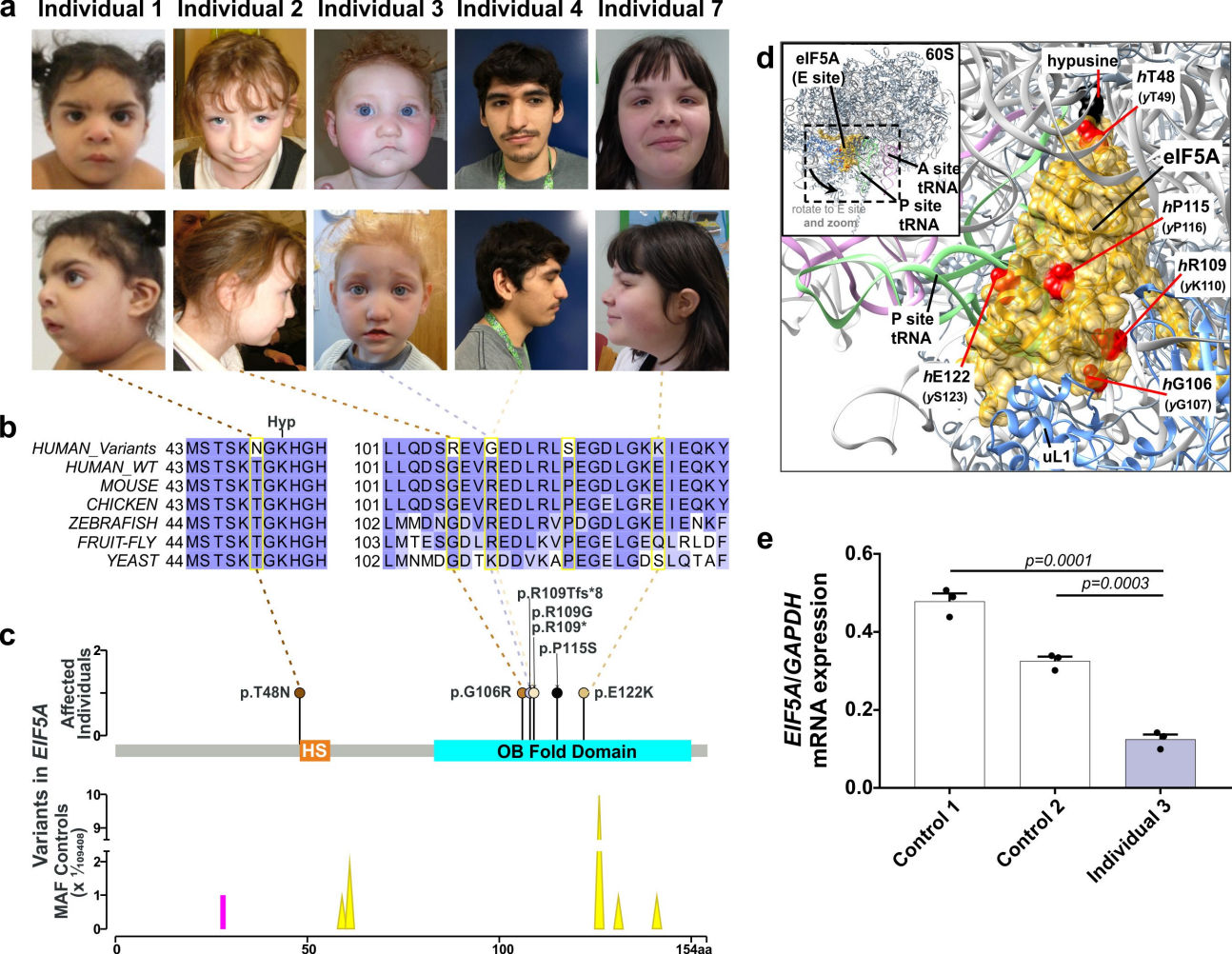
a
Individual 1
Individual 2
Individual 3
Individual 4
Individual 7
b
Hyp
HUMAN_Variants 43 MSTSKNGKHGH 101 LLQDSREVGEDLRLSEGDLGKKIEQKY
HUMAN_WT 43 MSTSKTGKHGH 101 LLQDSGEVREDLRLPEGDLGKEIEQKY
MOUSE 43 MSTSKTGKHGH 101 LLQDSGEVREDLRLPEGDLGKEIEQKY
CHICKEN 43 MSTSKTGKHGH 101 LLQDSGEVREDLRLPEGELGREIEQKY
ZEBRAFISH 44 MSTSKTGKHGH 102 LMMDNGDVREDLRVPDGDLGKEIENKF
FRUIT-FLY 44 MSTSKTGKHGH 103 LMTESGDLREDLKVPEGELGEQLRLDF
YEAST 44 MSTSKTGKHGH 102 LMNMDGDTKDDVKAPEGELGDSLQTAF
c
Affected Individuals
p.T48N
p.R109Tfs*8
p.R109G
p.R109*
p.P115S
p.G106R
p.E122K
HS
OB Fold Domain
Variants in EIF5A
MAF Controls (x 1/109408)
0
50
100
154aa
d
eIF5A (E site)
60S
A site tRNA
P site tRNA
rotate to E site and zoom
hypusine
hT48 (yT49)
eIF5A
hP115 (yP116)
hR109 (yK110)
P site tRNA
hE122 (yS123)
hG106 (yG107)
uL1
e
EIF5A/GAPDH mRNA expression
p=0.0001
p=0.0003
0.6
0.4
0.2
0.0
Control 1
Control 2
Individual 3

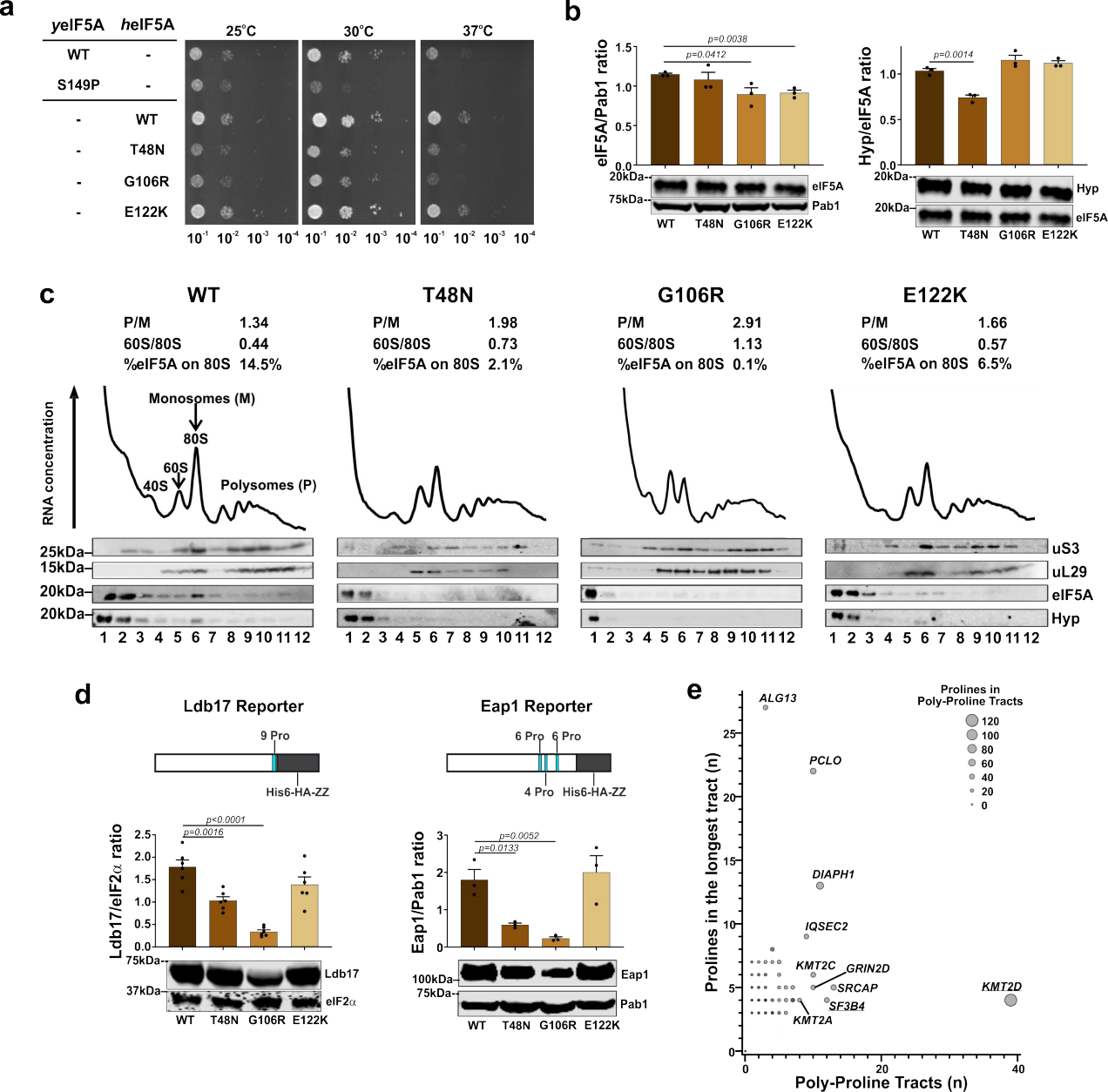
a
yeIF5A
heIF5A
WT
S149P
WT
T48N
G106R
E122K
25°C
30°C
37°C
b
eIF5A/Pab1 ratio
p=0.0038
p=0.0412
Hyp/eIF5A ratio
p=0.0014
eIF5A
Pab1
Hyp
WT
T48N
G106R
E122K
c
WT
T48N
G106R
E122K
P/M 1.34
60S/80S 0.44
%eIF5A on 80S 14.5%
P/M 1.98
60S/80S 0.73
%eIF5A on 80S 2.1%
P/M 2.91
60S/80S 1.13
%eIF5A on 80S 0.1%
P/M 1.66
60S/80S 0.57
%eIF5A on 80S 6.5%
RNA concentration
Monosomes (M)
80S
60S
40S
Polysomes (P)
uS3
uL29
eIF5A
Hyp
d
Ldb17 Reporter
9 Pro
His6-HA-ZZ
Eap1 Reporter
6 Pro 6 Pro
4 Pro His6-HA-ZZ
Ldb17/eIF2α ratio
p<0.0001
p=0.0016
Eap1/Pab1 ratio
p=0.0052
p=0.0133
Ldb17
eIF2α
Eap1
Pab1
WT
T48N
G106R
E122K
e
Prolines in Poly-Proline Tracts
ALG13
PCLO
DIAPH1
IQSEC2
KMT2C
GRIN2D
SRCAP
SF3B4
KMT2A
KMT2D
Prolines in the longest tract (n)
Poly-Proline Tracts (n)

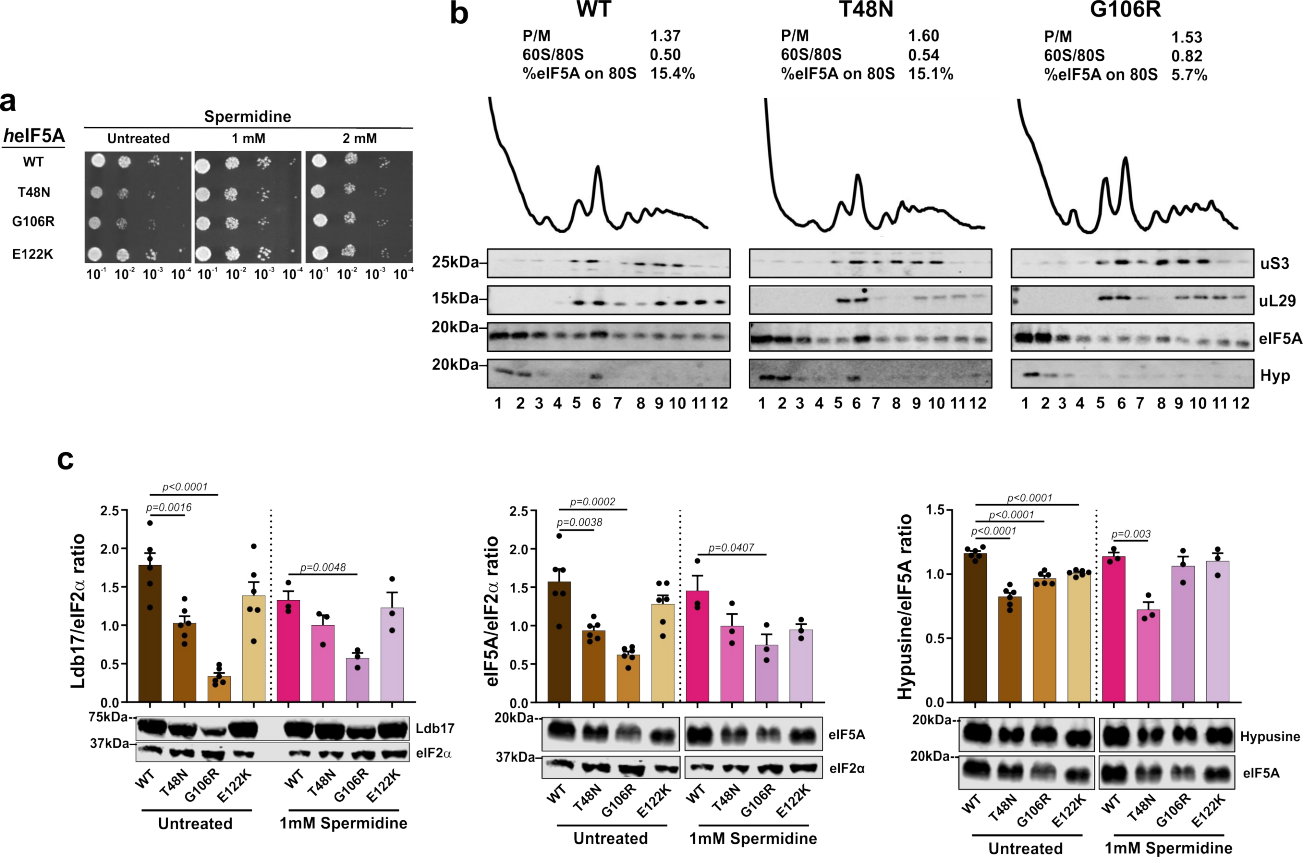
a
Spermidine
heIF5A
Untreated
1 mM
2 mM
WT
T48N
G106R
E122K
10-1 10-2 10-3 10-4
b
WT
P/M 1.37
60S/80S 0.50
%eIF5A on 80S 15.4%
T48N
P/M 1.60
60S/80S 0.54
%eIF5A on 80S 15.1%
G106R
P/M 1.53
60S/80S 0.82
%eIF5A on 80S 5.7%
25kDa
15kDa
20kDa
20kDa
uS3
uL29
eIF5A
Hyp
1 2 3 4 5 6 7 8 9 10 11 12
c
Ldb17/eIF2α ratio
p<0.0001
p=0.0016
p=0.0048
75kDa
37kDa
Ldb17
eIF2α
WT T48N G106R E122K WT T48N G106R E122K
Untreated
1mM Spermidine
eIF5A/eIF2α ratio
p=0.0002
p=0.0038
p=0.0407
20kDa
37kDa
eIF5A
eIF2α
Hypusine/eIF5A ratio
p<0.0001
p<0.0001
p<0.0001
p=0.003
20kDa
20kDa
Hypusine
eIF5A

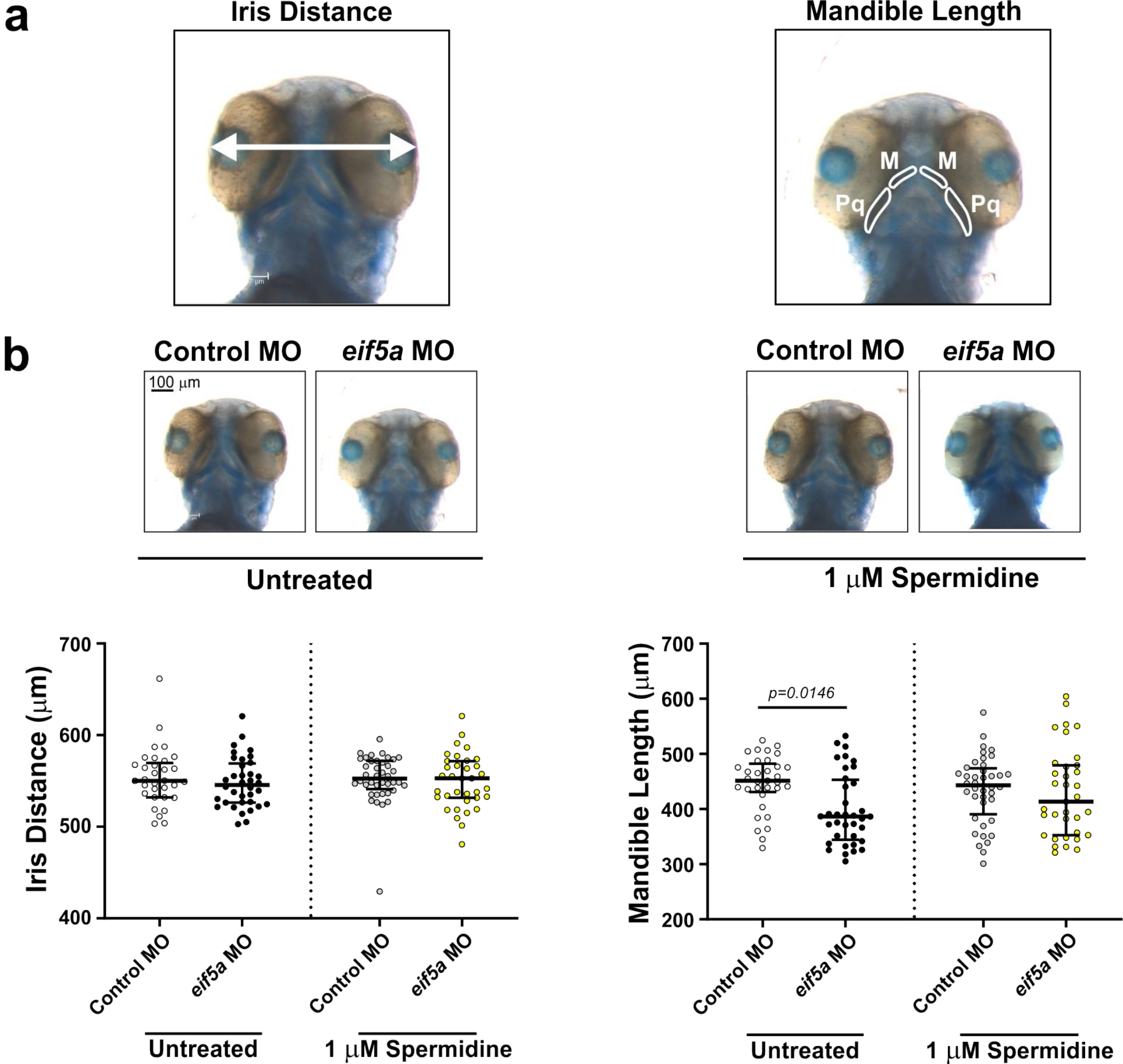
a
Iris Distance
Mandible Length
M
M
Pq
Pq
b
Control MO
eif5a MO
100 μm
Control MO
eif5a MO
Untreated
1 μM Spermidine
c
Iris Distance (μm)
700
600
500
400
Control MO
eif5a MO
Control MO
eif5a MO
Untreated
1 μM Spermidine
Mandible Length (μm)
700
600
500
400
300
200
p=0.0146
Control MO
eif5a MO
Control MO
eif5a MO
Untreated
1 μM Spermidine